IEEE Access
Multidisciplinary | Rapid Review | Open Access Journal

Received June 12, 2019, accepted July 4, 2019, date of publication July 9, 2019, date of current version July 26, 2019.

Digital Object Identifier 10.1109/ACCESS.2019.2927656

An Improved Grid-Search Method for the Identity-Test of Ionosphere-Layer Virtual Heights via TDOA Measurements

TIE-NAN ZHANG, XING-PENG MAO, (Member, IEEE), YU-GUAN HOU, AND HE MA

School of Electronics and Information Engineering, Harbin Institute of Technology, Harbin 150001, China
Key Laboratory of Marine Environmental Monitoring and Information Processing, Ministry of Industry and Information, Harbin Institute of Technology, Harbin 150001, China

Corresponding author: Xing-Peng Mao (mxp@ hit.edu.cn)

This work was supported by the Key Program of National Natural Science Foundation of China under Grant 61831009.

ABSTRACT Sky-wave time-difference-of-arrival (TDOA) localization is a promising technique, which may enable surveillance over large-scale areas via passive radar systems. In a recently published paper, we have proposed a novel sky-wave TDOA localization method by introducing an assumption, i.e., the ionosphere-layer virtual heights (IVHs) for transmitting paths from a target to different closely spaced sensors are identical. In this paper, we further verify the assumption by testing the identity of the IVHs based on TDOA measurements of a known-position target. To realize this goal, the identity-test problem is converted into a coefficient retrieval problem. The current state-of-the-art method has to make an approximation to select the nearest grid-point (NGP) of coefficient vector, which induces a larger recovery error with the increase of dimension. To alleviate this, an improved grid-search method is proposed by training weights, which can build the proportional relationship between the weighed norm-2 cost functions and the norm-2 distances of grid-points and coefficients. Thus, the NGP can be selected freely from the aforementioned approximation error; and the coefficient recovery accuracy is improved. Additionally, the training phase of the proposed method is guaranteed to be feasible while that of the conventional method is not. The simulation results verify the superiority of the proposed method over the current state-of-the-art in terms of recovery accuracy and computational complexity.

INDEX TERMS Nonlinear optimization, time-difference-of-arrival, sky-wave passive radar, ionosphere-layer virtual height.

I. INTRODUCTION

Time-difference-of-arrival (TDOA) localization is a passive localization technique which is widely applied in many applications [1]. Although line-of-sight (LOS) TDOA localization has been well-documented in the literature [2]–[6], non-line-of-sight (NLOS) TDOA localization is still an interesting topic that needs more research [7]–[9].

In this paper, our focus is a NLOS scenario where signals are reflected by the ionosphere-layer before arriving at sensors [10], [11]. The time delay of the transmitting path from a target to a sensor is equivalent to that of a spherical reflection path, with the height of the equivalent reflection point being the ionosphere-layer virtual height (IVH).

The associate editor coordinating the review of this manuscript and approving it for publication was Mehmet Alper Uslu.

Because an IVH is mainly determined by factors including signal frequency, ionosphere-layer status and the positions of source and sensor, it varies with time and is usually inaccurately known [10], [12]. Consequently, the inaccurately known IVHs can severely degrade TDOA localization performance. To alleviate this, we have introduced an assumption in [11] to propose a robust grid-search (RGS) method, i.e., the IVHs from a source to different sensors are identical when the maximum distance between these sensors is less than a threshold. In this paper, we further test the identity of IVHs, which is realized by solving a coefficient retrieval problem.

The inputs of the coefficient retrieval problem are TDOA measurements from an uncooperative target with its position known a priori. The outputs are coefficients which determine whether or not the IVHs are identical. The retrieval of coefficients from TDOA measurements is a nonlinear

optimization problem. As discussed in [11], due to the highly nonlinear relationship between TDOA measurements and coefficients, grid-search methods [13]–[17] are generally superior to parametric methods [18], [19]. Note that the grid-search methods for TDOA localization can be easily extended to solve the coefficient retrieval problem.

Conventional grid-search methods mainly consist of the compressed sensing (CS) methods and the norm-based methods. The former type includes bounded joint sparse (BJS) method [14], off-grid sparse Bayesian inference (OG-SBI) method [15] and single-target framework-based (SF) method [16]; and the latter type includes norm-2 method [17] and RGS method [11]. Besides, by converting the TDOA measurements into complex measurements [20], the multiple signal classification (MUSIC) method [21] is also applicable.

Despite RGS, the aforementioned methods do not guarantee that the nearest grid-point (NGP) of the coefficient vector can be found [11], which makes RGS a novel method in the current state-of-the-art. RGS works by: (a) dividing the scene-of-interest (SOI) into overlapping hyperspheres; (b) training a weight matrix to alleviate off-grid errors in an off-line process and (c) searching for the index of hypersphere where the coefficient vector is located. Then RGS estimates the NGP by making the approximation that selecting the right hypersphere (where the coefficient vector is located) is equivalent to selecting the NGP. A drawback of RGS is that this approximation induces a larger recovery error with the increase of dimension, which will be detailed afterwards. Another drawback of RGS is that its training phase is both time-consuming and not guaranteed to be feasible. These drawbacks imply that there is still room for improvements.

For this reason, as the main contribution of this paper, an improved grid-search method is proposed. On one hand, similar to RGS, the proposed method consists of an off-line weight training phase and an on-line searching phase. On the other hand, RGS requires that the low-order approximation is reasonable within a grid cell while the proposed method relies on a stronger assumption that the first-order approximation is reasonable in the whole SOI. Thus, by exploiting the structures of known first-order derivatives, a series of weights can be trained to build the proportional relationship between weighted norm-2 cost functions and the norm-2 distances of unknowns and grid-points. Therefore, the proposed method is named as the approximately proportional (AP) method, which does not need to divide the SOI into overlapping hyperspheres. AP avoids the approximation that selecting the right hypersphere is equal to selecting the NGP, which leads to coefficient recovery accuracy improvements. What's more, different from RGS, the training phase of AP is not only fast but also guaranteed to be feasible. In this way, the drawbacks of RGS are successfully alleviated.

The outline of this paper is as follows. In Section II, the measurement model, the coefficient retrieval problem and the conventional grid-search method are described. In Section III, the improved grid-search method is proposed. In Section IV and Section V, performance analyzes and simulation results are given, respectively. Conclusions are drawn in Section VI.

Notation: in this paper, bold symbols are reserved for vectors and matrices. $\boldsymbol{A}^{\mathrm{T}}$, $\boldsymbol{A}^{\dagger}$ and $\boldsymbol{A}^{-1}$ are the transpose, the pseudo-inverse and the inverse of matrix $\boldsymbol{A}$, respectively. vec$\{\cdot\}$ and tr$\{\cdot\}$ denote the vectorize and the trace notation, respectively. $||\boldsymbol{x}||_2$ represents the norm-2 of $\boldsymbol{x}$, $\mathbf{1}$ denotes a vector of all ones and $\boldsymbol{I}$ represents the identity matrix.

II. BASIC FUNDAMENTALS

A. MEASUREMENT MODEL

Consider the single-layer spherical reflection model as shown in Fig. 1, which is a widely used transmitting model in sky-wave localization [22], [23]. Then the time delay of the transmitting path from signal source (B) to sensor (A) is $\bar{AC} + \bar{BC}$, where C is the equivalent reflection point. The nearest distance between C and the earth surface is the IVH of transmitting path from B to A; and R_0 is the earth radius. By using the cosine theorem, we have

$$\bar{AC} = \bar{BC} = (\bar{OA}^2 + \bar{OC}^2 - 2\bar{OA}\bar{OC}\cos(\angle AOC))^{1/2} \quad (1)$$

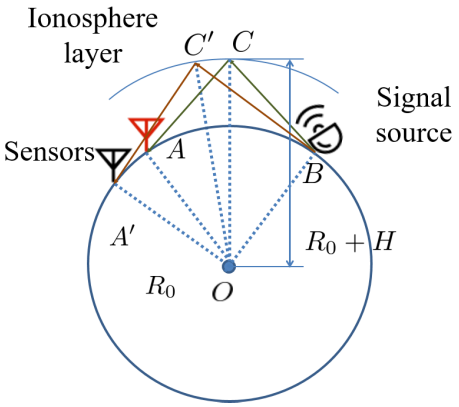

FIGURE 1. Illustration of spherical reflection paths from signal source to different sensors in sky-wave TDOA localization.

Suppose $\boldsymbol{s}_1, \cdots, \boldsymbol{s}_M$ are the known 3-D position vectors of M sensors and $\boldsymbol{u}$ is the known 3-D position vector of signal source. With $m = 1, \cdots, M$, define H_m the IVH for the path from $\boldsymbol{u}$ to $\boldsymbol{s}_m$, then the transmitting distance from $\boldsymbol{u}$ to $\boldsymbol{s}_m$ is

$$d_m = 2\sqrt{R_0^2 + (R_0 + H_m)^2 - 2R_0(R_0 + H_m)\sqrt{1 - \frac{L_m^2}{4R_0^2}}} \quad (2)$$

where $L_m = ||\boldsymbol{u} - \boldsymbol{s}_m||_2$. The range difference measured by $\boldsymbol{s}_m$ ($m \neq 1$) and $\boldsymbol{s}_1$ is

$$\tilde{d}_{m,1} = d_m - d_1 + c\Delta\tau_{m,1} \quad (3)$$

where $\Delta\tau_{m,1}$ is the measurement noise and c is the light speed. In this paper, it is assumed that $\Delta\tau_{2,1}, \cdots, \Delta\tau_{M,1}$ are independent identically distributed (i.i.d.) zero-mean Guassian noises, with σ_τ^2 being the identical variance.

Finally, stacking $\tilde{d}_{m,1}$ for $m = 2, \cdots, M$, we obtain the range difference measurement vector $\tilde{\boldsymbol{d}} \in \mathbb{R}^{(M-1)\times 1}$.

B. COEFFICIENT RETRIEVAL PROBLEM

In [11], we have introduced an assumption that $H_1, \cdots, H_M$ are identical when the maximum distance between $\boldsymbol{s}_1, \cdots, \boldsymbol{s}_M$ is less than a threshold (30-100 km), which is termed as A1. A1 can be supported by [24], where Bourgeois claimed that the IVH from a moving target to a static sensor barely changes within 20 minutes, with the target speed being around 100 m/s. Therefore the IVHs from a static sensor to different positions in the trajectory are approximately identical and A1 is supported. Similarly, the IVH from a moving target to a static sensor is assumed to change intermittently in [10], which also supports A1.

The aim of this paper is to test the identity of IVHs via the TDOA measurements of a known-position target. To achieve this, it is straightforward to retrieve $H_1, \cdots, H_M$ from $\tilde{\boldsymbol{d}}$. However, this problem is under-determined. For this reason, we next introduce ionosphere-layer status coefficients to transform the identity-test problem into a coefficient retrieval problem. The appropriateness of the constructed coefficient retrieval problem will also be discussed.

To start with, assume that the ionosphere-layer stays constant during the observation time and that H_m is the elementary function of $\boldsymbol{u}$ and $\boldsymbol{s}_m$ (expressed as $f(\boldsymbol{u}, \boldsymbol{s}_m)$). Applying Taylor expansions, then H_m and H_1 satisfy

$$H_m = H_1 + \sum_{i=1}^{3}\sum_{j=0}^{\infty} c_{m,i,j}(s_m(i,1) - s_1(i,1))^j \tag{4}$$

where $c_{m,i,j}$ represents an ionosphere-layer status coefficient.

Because the sensors are on the earth surface, $s_m(3,1)$ is the function of $s_m(1,1)$ and $s_m(2,1)$. Then (4) changes into

$$H_m = H_1 + \sum_{i=1}^{2}\sum_{j=0}^{\infty} \bar{c}_{m,i,j}(s_m(i,1) - s_1(i,1))^j \tag{5}$$

Further assume that, when the maximum distance between sensors is less than a threshold (30-100 km), the coefficients are identical for different m ($c_{i,j} = \bar{c}_{1,i,j} = \cdots = \bar{c}_{M,i,j}$). Then

$$H_m = H_1 + \sum_{i=1}^{2}\sum_{j=0}^{\infty} c_{i,j}(s_m(i,1) - s_1(i,1))^j \tag{6}$$

If the analytical expression of $f(\boldsymbol{u}, \boldsymbol{s}_m)$ is known, then (6) can be approximated by several Taylor expansion terms. However, the derivation of the analytical expression is very complicated and requires future research. Alternatively, we can retain the former $2N$ Taylor expansion terms in (6) as long as the retrieval problem is over-determined ($2N \leq M-1$). When M is large enough, N could be large enough to make the approximation appropriate.

For simplicity, we only retain the first-order terms in this paper, leading to a weaker assumption of A1, i.e.,

$$H_m - H_1 \approx c_1(s_m(1,1) - s_1(1,1)) + c_2(s_m(2,1) - s_1(2,1)) \tag{7}$$

Because H_1 is generally inaccurately known or unknown, the retrieval problem is to estimate H_1, c_1 and c_2 via $\tilde{\boldsymbol{d}}$.

The appropriateness of the constructed coefficient retrieval problem can be observed by noting that $c_1 = c_2 = 0$ is the sufficient and necessary condition of $H_1 = \cdots = H_M$ when the matrix below is full rank in column, i.e.,

$$\boldsymbol{P} = \left[-\mathbf{1}_{M-1\times 1}, \boldsymbol{I}_{(M-1)\times(M-1)}\right] \begin{bmatrix} s_1(1,1) & s_1(2,1) \\ s_2(1,1) & s_2(2,1) \\ \vdots & \vdots \\ s_M(1,1) & s_M(2,1) \end{bmatrix} \tag{8}$$

which satisfies $[H_2 - H_1, \cdots, H_M - H_1]^{\mathrm{T}} = \boldsymbol{P}[c_1, c_2]^{\mathrm{T}}$. This means the XY coordinates of sensors should not be in the same line. Due to this, we will use the typical scenario in Fig. 2 for coefficient retrieval.

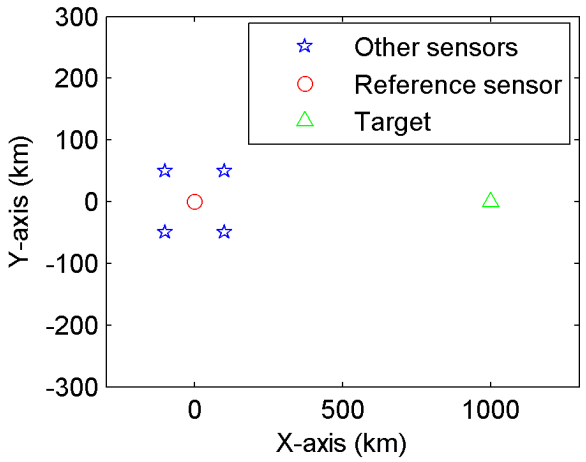

FIGURE 2. Deployment of sensor geometry for coefficient retrieval.

C. CONVENTIONAL GRID-SEARCH METHODS

In [11], it has been shown that using parametric methods is generally inefficient to retrieve information from $\tilde{\boldsymbol{d}}$ because of the highly nonlinear relationship between $\tilde{\boldsymbol{d}}$ and unknowns. Hence, grid-search methods are preferred in [11]. Following this, we retrieve c_1 and c_2 from $\tilde{\boldsymbol{d}}$ via grid-search methods. Next we briefly review the RGS method proposed in [11], which is a grid-search method that can approximately select the NGP of unknowns.

Recall that the unknowns include c_1, c_2 and H_1. When the rough ranges of unknowns are given, grid-points can be generated by dividing the 3D space into G grid-points. Without loss of generality, we suppose there are G_{sub} grid-points in each axis. Then we obtain $G = G_{\mathrm{sub}}^3$ grid-points $\boldsymbol{r}_1, \cdots, \boldsymbol{r}_G$.

Define SOI as the bounded 3D search space, then RGS works by dividing the SOI into overlapping hyperspheres. To achieve this, it needs to divide the SOI into cubes [11]. However, the ranges of H_1 and c_1 (c_2) are generally different, which makes it hard to obtain the required cubes.

Section III-A will propose a trick to generate the required cubes, which transforms $\boldsymbol{r}_1, \cdots, \boldsymbol{r}_G$ into $\bar{\boldsymbol{r}}_1, \cdots, \bar{\boldsymbol{r}}_G$; and $\bar{\boldsymbol{r}}_g$ is

used hereafter. Then $\bar{\boldsymbol{r}}$ is the unknown vector to be retrieved and $\bar{\Psi}_g = \{\bar{\boldsymbol{r}} | ||\bar{\boldsymbol{r}} - \bar{\boldsymbol{r}}_g||_2 \leq \sqrt{D}\rho/2\}$ for all g are the overlapping hyperspheres, with D the dimension of SOI and ρ the side length of cube. The TDOA measurements generated by $\bar{\boldsymbol{r}}_1, \cdots, \bar{\boldsymbol{r}}_G$ are $\boldsymbol{d}^1, \cdots, \boldsymbol{d}^G$.

Then RGS builds the sufficient condition for the selection of hypersphere where $\bar{\boldsymbol{r}}$ is located, which is related with the training of a weight matrix $\boldsymbol{W}$. The training process relies on a convex optimization process, i.e.,

$$\max_{\boldsymbol{W}} \ \eta$$
$$\text{s.t.} \begin{cases} 8 \max\limits_{g} \{\rho_D^2 \text{tr}\{(\delta\bar{\boldsymbol{\Phi}}^g)^{\text{T}} \boldsymbol{W} \delta\bar{\boldsymbol{\Phi}}^g\} \\ +\rho_D^4 \text{tr}\{(\delta\bar{\boldsymbol{\Theta}}^g)^{\text{T}} \boldsymbol{W} \delta\bar{\boldsymbol{\Theta}}^g\}\} \leq \eta \\ \eta < \min\limits_{g,g' | g \neq g'} \text{tr}\{(\boldsymbol{d}^g - \boldsymbol{d}^{g'})(\boldsymbol{d}^g - \boldsymbol{d}^{g'})^{\text{T}} \boldsymbol{W}\} \\ \boldsymbol{W} \succeq \boldsymbol{0} \\ \text{tr}\{\boldsymbol{W}\} \leq 1 \end{cases} \tag{9}$$

where $\rho_D = \sqrt{D}\rho/2$, $\Delta\bar{\boldsymbol{r}}_g = \bar{\boldsymbol{r}} - \bar{\boldsymbol{r}}_g$, $\delta\bar{\boldsymbol{\Phi}}^g$ and $\delta\bar{\boldsymbol{\Theta}}^g$ are the first and second derivative matrices which satisfy

$$\boldsymbol{d} - \boldsymbol{d}^g \approx \delta\bar{\boldsymbol{\Phi}}^g \Delta\bar{\boldsymbol{r}}_g + \delta\bar{\boldsymbol{\Theta}}^g \text{vec}\{\Delta\bar{\boldsymbol{r}}_g \Delta\bar{\boldsymbol{r}}_g^{\text{T}}\} \tag{10}$$

It is worth noting that RGS makes the low-order approximation only between $\bar{\boldsymbol{r}}$ and the NGP of $\bar{\boldsymbol{r}}$; and the training phase of RGS is off-line because it is not dependent on $\tilde{\boldsymbol{d}}$.

The searching phase of RGS is

$$\arg\min_{g} \left|\left|(\tilde{\boldsymbol{d}} - \boldsymbol{d}^g)^{\text{T}} \boldsymbol{W} (\tilde{\boldsymbol{d}} - \boldsymbol{d}^g)\right|\right|_2^2 \tag{11}$$

which can generally lead to the right hypersphere $\bar{\Psi}_g$ when measurement noises are small enough.

However, RGS has to make the approximation that selecting the right $\bar{\Psi}_{g1}$ leads to $||\bar{\boldsymbol{r}} - \bar{\boldsymbol{r}}_{g1}||_2 = \min\limits_{g} ||\bar{\boldsymbol{r}} - \bar{\boldsymbol{r}}_g||_2$. If the 3D grid-search problem reduces to a 2-D one, the approximation is reasonable because $\rho_D = \sqrt{2}\rho/2$ makes $\bar{\boldsymbol{r}}$ located in at most two hyperspheres. Thus $\bar{\boldsymbol{r}}_{g1}$ is the NGP or the second NGP of $\bar{\boldsymbol{r}}$; and using the approximation $||\bar{\boldsymbol{r}} - \bar{\boldsymbol{r}}_{g1}||_2 \approx \min\limits_{g} ||\bar{\boldsymbol{r}} - \bar{\boldsymbol{r}}_g||_2$ will induce a small error. But in 3D grid-search, $\bar{\boldsymbol{r}}$ can be located in more hyperspheres, which may lead to a larger approximation error. With the increase of D, $\bar{\boldsymbol{r}}_{g1}$ can be the kth NGP, where $k \gg 1$. This can make the approximation error very large, which is the first drawback of RGS.

Another drawback of RGS is that it has a training phase which is not only quite time-consuming (due to the second inequality in (9)) but also not guaranteed to be feasible.

III. THE PROPOSED METHOD

A. APPROXIMATELY PROPORTIONAL METHOD

Similar to RGS, the proposed method also requires the rough ranges of unknowns. More importantly, because the ranges of c_1, c_2 and H_1 are different, a simple trick is used to divide the 3D search space into the required cubes by transforming $\boldsymbol{r}_g$ into $\bar{\boldsymbol{r}}_g$. Suppose the range of H_1 is $[H_{1,L}, H_{1,U}]$ and the identical range of c_1 and c_2 is $[c_L, c_U]$. The unknown vector can be defined by $\bar{\boldsymbol{r}} = [Qc_1, Qc_2, H_1]$, with $Q = (H_{1,U} - H_{1,L})/(c_U - c_L)$. Then the required uniform grid-points can be generated by

$$\bar{\boldsymbol{r}}_g = \begin{bmatrix} Qc_L + k_1\rho \\ Qc_L + k_2\rho \\ H_{1,L} + k_3\rho \end{bmatrix} \tag{12}$$

where $k_1, k_2, k_3 = 0, 1, \cdots, G_{\text{sub}} - 1$, with $G_{\text{sub}} = (H_{1,U} - H_{1,L})/\rho = G^{1/3}$.

Next, we consider the noise-free measurement vector $\boldsymbol{d}$. We propose to train the weight for $\boldsymbol{d} - \boldsymbol{d}^g$ to build the approximately proportional relationship between $(\boldsymbol{d} - \boldsymbol{d}^g)^{\text{T}} \bar{\boldsymbol{W}}_g (\boldsymbol{d} - \boldsymbol{d}_g)$ and $||\Delta\bar{\boldsymbol{r}}_g||_2$, with the weight being $\bar{\boldsymbol{W}}_g$. To achieve this, we make the approximation that $\boldsymbol{d} - \boldsymbol{d}^g \approx \delta\bar{\boldsymbol{\Phi}}^g \Delta\bar{\boldsymbol{r}}_g$ in the whole SOI. Further define $\bar{\boldsymbol{W}}_g = ((\delta\bar{\boldsymbol{\Phi}}^g)^{\dagger})^{\text{T}} (\delta\bar{\boldsymbol{\Phi}}^g)^{\dagger}$, then

$$\begin{aligned} \left|\left|\boldsymbol{d} - \boldsymbol{d}^g\right|\right|_{\bar{\boldsymbol{W}}_g}^2 &\overset{\text{def}}{=} (\boldsymbol{d} - \boldsymbol{d}_g)^{\text{T}} \bar{\boldsymbol{W}}_g (\boldsymbol{d} - \boldsymbol{d}_g) \\ &\approx \bar{\boldsymbol{r}}_g^{\text{T}} (\delta\bar{\boldsymbol{\Phi}}^g)^{\text{T}} ((\delta\bar{\boldsymbol{\Phi}}^g)^{\dagger})^{\text{T}} (\delta\bar{\boldsymbol{\Phi}}^g)^{\dagger} \delta\bar{\boldsymbol{\Phi}}^g \bar{\boldsymbol{r}}_g \end{aligned} \tag{13}$$

Assume $\delta\bar{\boldsymbol{\Phi}}^g$ is full rank in column for all $\boldsymbol{g}$, then

$$\left|\left|\boldsymbol{d} - \boldsymbol{d}^g\right|\right|_{\bar{\boldsymbol{W}}_g}^2 \approx ||\Delta\bar{\boldsymbol{r}}_g||_2^2 \tag{14}$$

Finally, after generating $\bar{\boldsymbol{W}}_1, \cdots, \bar{\boldsymbol{W}}_G$ by $\delta\bar{\boldsymbol{\Phi}}^1, \cdots, \delta\bar{\boldsymbol{\Phi}}^G$, the searching process is

$$\arg\min_{g} \left|\left|\boldsymbol{d} - \boldsymbol{d}^g\right|\right|_{\bar{\boldsymbol{W}}_g}^2 \tag{15}$$

Obviously, when the NGP of $\bar{\boldsymbol{r}}$ is $\bar{\boldsymbol{r}}_{g1}$, $||\bar{\boldsymbol{r}}_{g1}||_2 < ||\bar{\boldsymbol{r}}_{g2}||_2$ holds for all $g2 \neq g1$, with $g2 = 1, \cdots, G$. This leads to $g1 = \arg\min\limits_{g} \left|\left|\boldsymbol{d} - \boldsymbol{d}^g\right|\right|_{\bar{\boldsymbol{W}}_g}^2$.

B. IMPACT OF MEASUREMENT NOISE

When dealing with the noisy measurement vector $\tilde{\boldsymbol{d}}$, we propose to solve the optimization problem below

$$\arg\min_{g} \left|\left|\tilde{\boldsymbol{d}} - \boldsymbol{d}^g\right|\right|_{\bar{\boldsymbol{W}}_g}^2 \tag{16}$$

Next we will show that (16) can lead to neighborhood grid-points around $\bar{\boldsymbol{r}}$ or the NGP when $\sigma_d = c\sigma_\tau \ll \rho$. The concept of neighborhood grid-point is explained in Fig. 3.

Firstly, with $\tilde{\boldsymbol{d}} = \boldsymbol{d} + \Delta\boldsymbol{d}$, we have

$$\begin{aligned} \left|\left|\tilde{\boldsymbol{d}} - \boldsymbol{d}^g\right|\right|_{\bar{\boldsymbol{W}}_g}^2 &\approx ||\Delta\bar{\boldsymbol{r}}_g||_2^2 \\ &+ \Delta\boldsymbol{d}^{\text{T}} \bar{\boldsymbol{W}}_g \Delta\boldsymbol{d} + 2\Delta\boldsymbol{d}^{\text{T}} \bar{\boldsymbol{W}}_g \Delta\bar{\boldsymbol{r}}_g \end{aligned} \tag{17}$$

Let $\bar{\boldsymbol{r}}_{g1}$ be the NGP (of $\bar{\boldsymbol{r}}$) and $\bar{\boldsymbol{r}}_{g2}$ be a grid-point which is neither the NGP nor a neighborhood grid-point. Now the task is to prove that

$$\left|\left|\tilde{\boldsymbol{d}} - \boldsymbol{d}^{g1}\right|\right|_{\bar{\boldsymbol{W}}_{g1}}^2 < \left|\left|\tilde{\boldsymbol{d}} - \boldsymbol{d}^{g2}\right|\right|_{\bar{\boldsymbol{W}}_{g2}}^2 \tag{18}$$

Eq. (18) is the sufficient and necessary condition of

$$\begin{aligned} 2\Delta\boldsymbol{d}^{\text{T}} (\bar{\boldsymbol{W}}_{g1} \Delta\bar{\boldsymbol{r}}_{g1} - \bar{\boldsymbol{W}}_{g2} \Delta\bar{\boldsymbol{r}}_{g2}) &< ||\Delta\bar{\boldsymbol{r}}_{g2}||_2^2 - ||\Delta\bar{\boldsymbol{r}}_{g1}||_2^2 \\ &+ \Delta\boldsymbol{d}^{\text{T}} \bar{\boldsymbol{W}}_{g1} \Delta\boldsymbol{d} - \Delta\boldsymbol{d}^{\text{T}} \bar{\boldsymbol{W}}_{g2} \Delta\boldsymbol{d} \end{aligned} \tag{19}$$

Secondly, following the 3σ principle, with the probability close to 1, $||\Delta \boldsymbol{d}||_2^2 \leq 9(M-1)\sigma_d^2$. Recall that $\bar{\boldsymbol{W}}_g$ is semi-definite positive, then the sufficient condition of (19) is

$$6\sqrt{M-1}\sigma_d\lambda_{12}(||\Delta\bar{\boldsymbol{r}}_{g1}||_2+||\Delta\bar{\boldsymbol{r}}_{g2}||_2) +9(M-1)\sigma_d^2\lambda_{\max}\{\bar{\boldsymbol{W}}_{g2}\}<||\Delta\bar{\boldsymbol{r}}_{g2}||_2^2-||\Delta\bar{\boldsymbol{r}}_{g1}||_2^2 \quad (20)$$

where $\lambda_{12}=\max\{\lambda_{\max}\{\bar{\boldsymbol{W}}_{g1}\},\lambda_{\max}\{\bar{\boldsymbol{W}}_{g2}\}\}$ and $\lambda_{\max}\{\bar{\boldsymbol{W}}\}$ denotes the largest eigenvalue of $\bar{\boldsymbol{W}}$.

We set $\sigma_\tau \leq 100$ ns in this paper, which is a common parameter range of σ_τ in sky-wave TDOA localization [11]. Hence $\sigma_d \ll 1$ km and the second term on the left hand side of (20) is ignorable compared with the first term thereof. The sufficient condition of (20) changes into

$$6\sqrt{M-1}\sigma_d\lambda_{12}<||\Delta\bar{\boldsymbol{r}}_{g2}||_2-||\Delta\bar{\boldsymbol{r}}_{g1}||_2 \quad (21)$$

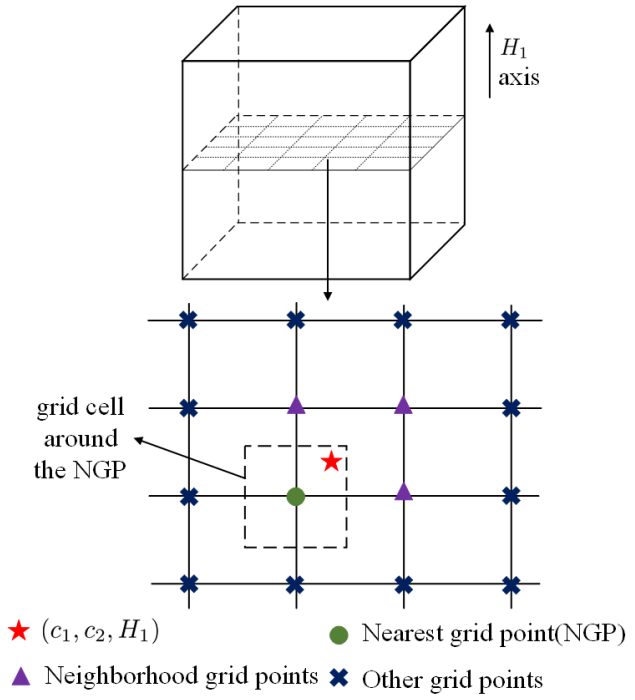

FIGURE 3. Illustration of uniform grids in (c_1, c_2, H_1) space and (c_1, c_2) plane.

Finally, it can be observed from Fig. 3 that $||\bar{\boldsymbol{r}}_{g2}||_2 - ||\bar{\boldsymbol{r}}_{g1}||_2 \geq \rho$ approximately holds when $\bar{\boldsymbol{r}}_{g1}$ is the NGP and $\bar{\boldsymbol{r}}_{g2}$ is neither a neighborhood grid-point nor the NGP. Hence, (18) holds when $\rho \gg \sigma_d$. In other words, $g=\arg\min_g \left|\left|\tilde{\boldsymbol{d}}-\boldsymbol{d}^g\right|\right|^2_{\bar{\boldsymbol{W}}_g}$ should be the index of NGP or a neighborhood grid-point.

Additionally, if we deem $\bar{\boldsymbol{r}}$ as a random variable which is uniformly distributed within the grid cell around NGP, then the lower-bound of the probability of success to select $\bar{\boldsymbol{r}}_{g1}$ (when $\bar{\boldsymbol{r}}_{g1}$ is the NGP) can be calculated by

$$\mathrm{P}_{s,\bar{\boldsymbol{r}}_{g1}}=\prod_{i\neq g_1}\mathrm{P}(6\sqrt{M-1}\sigma_d\lambda_{1i}<||\Delta\bar{\boldsymbol{r}}_{gi}||_2-||\Delta\bar{\boldsymbol{r}}_{g1}||_2) \quad (22)$$

Although the analytical calculation of $\mathrm{P}_{s,\bar{\boldsymbol{r}}_{g1}}$ is very complicated, $\mathrm{P}_{s,\bar{\boldsymbol{r}}_{g1}}$ can be calculated via a numerical process. This is achieved by dividing the grid cell around $\bar{\boldsymbol{r}}_{g1}$ into $\bar{G}$ dense points $(\bar{\boldsymbol{r}}_{g1,1},\cdots,\bar{\boldsymbol{r}}_{g1,\bar{G}})$. If there are $\bar{N}$ points which satisfy the $G-1$ inequalities in (22), then $\mathrm{P}_{s,\bar{\boldsymbol{r}}_{g1}}\approx\bar{N}/\bar{G}$.

As an example, we calculate $\mathrm{P}_{s,\bar{\boldsymbol{r}}_{g1}}$ for the 3D grid cell around $\bar{\boldsymbol{r}}_{g1}=[-155.55,-155.55,144.44]$, with $[c_L,c_U]=[-1,1]$; and other simulation conditions are the same with those of Section V-B. The results are depicted in Table 1 and it is shown that the values of $\mathrm{P}_{s,\bar{\boldsymbol{r}}_{g1}}$ obtained by numerical calculation are close to those obtained by simulation tests in the interested range of σ_τ ($\sigma_\tau \leq 100$ ns).

TABLE 1. The percentages of success to select the NGP obtained by derivation and simulation.

σ_τ	10 ns	10^2 ns	10^3 ns	10^4 ns
The derived percentage of success	89.19%	72.33%	34.43%	0%
The actual percentage of success	94.2%	94.2%	93.7%	72.9%

What's more, it can be observed from (22) that $\mathrm{P}_{s,\bar{\boldsymbol{r}}_{g1}}$ is a monotonically decreasing function of λ_{1i}. This means using the weighed norm-2 functions to alleviate off-grid errors makes the proposed method more sensitive to measurement noises than using norm-2 functions, with $\lambda_{1i}\geq 1$.

Algorithm 1 The Proposed Method

Require: The TDOA measurement vector $\tilde{\boldsymbol{d}}$, the grid-points $\boldsymbol{r}_1,\cdots,\boldsymbol{r}_G$.

1: Training phase
Calculate uniform grid-points $\bar{\boldsymbol{r}}_1,\cdots,\bar{\boldsymbol{r}}_G$ and the corresponding first-order derivatives $\delta\bar{\boldsymbol{\Phi}}^1,\cdots,\delta\bar{\boldsymbol{\Phi}}^G$ via (12). Calculate $\bar{\boldsymbol{W}}_1,\cdots,\bar{\boldsymbol{W}}_G$ which are defined above (13).

2: Searching phase
Calculate $g1=\arg\min_g ||\tilde{\boldsymbol{d}}-\boldsymbol{d}^g||^2_{\bar{\boldsymbol{W}}_g}$, output $\boldsymbol{r}_{g1}$.

IV. DISCUSSION AND PERFORMANCE ANALYSIS

A. ADVANTAGES AND LIMITATIONS

The advantages of the proposed method are two-fold. Firstly, it does not need to divide the SOI into hyperspheres, which fixes the first drawback of RGS. Secondly, its training process consists of G pseudo-inverse procedures which are always feasible, thus alleviating the second drawback of RGS. Section IV-B will further verify that the training process of AP is much faster than that of RGS.

The limitation of the proposed method is that it makes first-order approximations within the whole SOI, while RGS approximates $\boldsymbol{d}-\boldsymbol{d}^g$ with its first and second-order Taylor expansions only when $\boldsymbol{r}^g$ is the NGP. Hence, the proposed method should suffer from more Taylor approximation errors. Fortunately, the ranges of c_1 and c_2 should be small by recalling the maximum distance between sensors and the limited range of IVH. Section IV-C will show that the first-order

approximation is appropriate when the ranges of c_1 and c_2 are smaller than $[-5, 5]$, which should be the maximum scales of c_1 and c_2 in most cases.

B. ANALYSIS OF COMPUTATIONAL COMPLEXITY

The training phase of RGS relies on a convex optimization process which deals with a $G(G-1)/2$ dimension matrix according to (9). For this reason, the training process of RGS is quite time-consuming. Alternatively, the training process of the proposed method is much faster. It consists of G pseudo-inverse procedures, corresponding to $\delta\bar{\boldsymbol{\Phi}}^1, \cdots, \delta\bar{\boldsymbol{\Phi}}^G$, respectively. The dimension of $\delta\bar{\boldsymbol{\Phi}}^g$ is $(M-1)\times D$, leading to the computational complexity of $\mathcal{O}((M-1)^3G)$. For verification, the CPU run-time test results are depicted in Table 2. Expect G, the simulation conditions of Section V-B are used in this subsection.

TABLE 2. CPU run-time tests of the training processes of RGS and the proposed method.

G	RGS (s)	The proposed method (s)
216	2.257	0.081
343	3.651	0.106
512	9.129	0.156
729	20.917	0.224
1000	55.269	0.307
1331	106.730	0.406

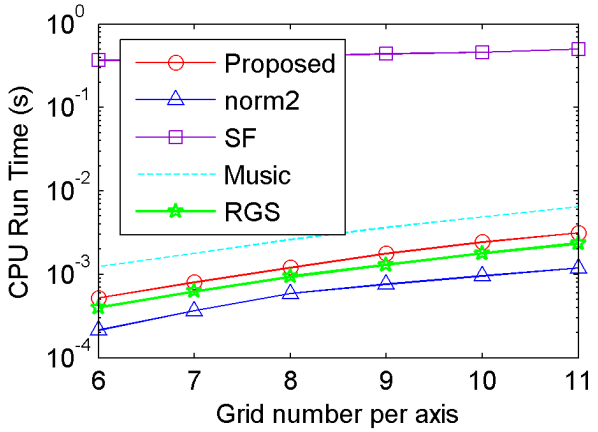

FIGURE 4. CPU run-time versus the grid number per axis.

Additionally, in [11], we have shown that the searching phase of RGS is very computationally cheap, with the computational complexity being $\mathcal{O}((M-1)^2G)$. The searching phase of the proposed method also needs the computational complexity of $\mathcal{O}((M-1)^2G)$ according to (16). Hence, the proposed method is also a fast grid-search method. To verify this, Fig. 4 is used to compare the proposed method with other grid-search methods. It is shown that the CPU run-time cost of AP is close to that of RGS.

C. RELATIONSHIP BETWEEN THE PROPOSED METHOD AND TAYLOR SERIES

Taylor series [25], [26] (TS) is a classical iterative method which is well-known to be locally optimal. Similar to the proposed method, it utilizes the first-order approximation within the whole SOI. The contents to follow will show that: (a) TS equivalently minimizes a norm-2 cost function which is different from the proposed method and (b) the proposed method is less affected by local minimums compared with TS.

(a) Note that TS does not need to transform $\boldsymbol{r}$ into $\bar{\boldsymbol{r}}$. Let $\boldsymbol{r}^k|_{k=0}$ be the initial guess of $\boldsymbol{r}$ and $\boldsymbol{r}^k|_{k=1,\cdots}$ be the intermediate results of TS. Define $\delta\boldsymbol{\Phi}(\boldsymbol{r}^k)$ and $\boldsymbol{d}(\boldsymbol{r}^k)$ the first-order derivative matrix and the data vector calculated by $\boldsymbol{r}^k$, respectively. Then the first-order approximation made in the kth iteration of TS is

$$\tilde{\boldsymbol{d}} \approx \boldsymbol{d}(\boldsymbol{r}^k) + \delta\boldsymbol{\Phi}(\boldsymbol{r}^k)(\boldsymbol{r}-\boldsymbol{r}^k) + \Delta\boldsymbol{d} \tag{23}$$

Then TS calculates $\boldsymbol{r}$ by solving

$$\min_{\boldsymbol{r}} ||\tilde{\boldsymbol{d}} - \boldsymbol{d}(\boldsymbol{r}^k) - \delta\boldsymbol{\Phi}(\boldsymbol{r}^k)(\boldsymbol{r}-\boldsymbol{r}^k)||_2^2 \tag{24}$$

By solving (24), the updating rule for the kth ($k = 1, \cdots$) iteration is given by

$$\boldsymbol{r}^{k+1} = \boldsymbol{r}^k - \lambda\delta\boldsymbol{\Phi}^\dagger(\boldsymbol{r}^k)(\tilde{\boldsymbol{d}} - \boldsymbol{d}(\boldsymbol{r}^k)) \tag{25}$$

where λ is the updating step which is usually empirically determined. The iteration process stops when a given threshold ζ satisfies

$$\zeta \geq ||\boldsymbol{r}^{k+1} - \boldsymbol{r}^k||_2 / ||\boldsymbol{r}^k||_2 \tag{26}$$

The optimization problem in (24) can be converted into

$$\min_{\boldsymbol{r}} ||\Delta\boldsymbol{d}||_2^2 \tag{27}$$

Further convert (15) into $\min_g ||\Delta\bar{\boldsymbol{r}}_g||_2^2$, then the difference between cost functions can be observed: TS is based on the maximum likelihood criterion and AP is based on the minimum off-grid error criterion.

(b) TS works by iteratively updating $\boldsymbol{r}$ and is likely to convey when an intermediate result is near a local minimum. Alternatively, AP works by minimizing $||\Delta\bar{\boldsymbol{r}}_g||_2^2$, which is actually a convex problem. Although the first order approximation made in AP may make $\left|\left|\boldsymbol{d} - \boldsymbol{d}^g\right|\right|_{\bar{\boldsymbol{W}}_g}^2$ smaller than $||\Delta\bar{\boldsymbol{r}}_g||_2^2$ and thus causes local minimums, AP is still less sensitive to local minimums than TS. The reason is as follows. When the grid-points are dense enough so that $\bar{\boldsymbol{r}}$ coincides with its NGP ($\bar{\boldsymbol{r}}_{g1}$), $||\boldsymbol{d} - \boldsymbol{d}(\bar{\boldsymbol{r}}_{g1})||_{\bar{\boldsymbol{W}}_{g1}}^2 = 0$. This implies that the cost function generated by NGP is at least no larger than the cost functions generated by the grid-points around local minimums. Thus, the grid-points near the local minimums are not necessarily selected, which means the proposed method is less affected by the local optimums than TS.

What's more, another difference between TS and AP is that AP avoids the selection of updating step and conveying threshold, making the usage of AP more convenient in practice.

To verify the superiority of AP over TS, we utilize the simulation conditions in Section V-B to obtain the results in Fig. 5. In this figure, T1, T2, T3 and T4 correspond to four test conditions, i.e., $(\lambda, \zeta) = (10^{-4}, 10^{-3})$,

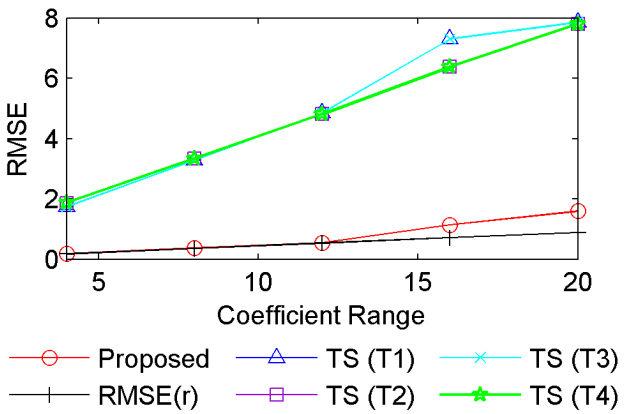

FIGURE 5. RMSE versus coefficient range in terms of the proposed method and TS under different test conditions.

$(\lambda, \zeta) = (10^{-3}, 10^{-3})$, $(\lambda, \zeta) = (10^{-4}, 10^{-4})$ and $(\lambda, \zeta) = (10^{-3}, 10^{-4})$, respectively. The definition of root mean square error (RMSE) is given in Section V; and RMSE(r) is the lower bound of RMSE generated by the NGP.

It is observed from Fig. 5 that the proposed method keeps behaving better than TS under four test conditions, which verifies the superiority of AP. A by-product is that the first-order approximation error barely affects the proposed method when the identical range of c_1 and c_2 is smaller than $[-5, 5]$, which should be the maximum scale of c_1 and c_2 in most cases.

V. SIMULATION RESULTS

As parameter settings of this section, $R_0 = 6378$ km and the identical range of c_1 and c_2 is $[-0.1, 0.1]$. The XY coordinates of sensors and target are depicted in Fig. 2. In Section V-A, H_1 is assumed to be known ($H_1 = 200$ km), leading to a 2D grid-search problem. In Section V-B, H_1 is unknown, leading to a 3D grid-search problem; and the rough range of H_1 is set to [100, 500] km according to the property of ionosphere-layer.

Besides, according to [27], the calculation of σ_τ based on signal-to-noise ratio (SNR) is

$$\sigma_\tau^2 = \frac{3T_s^2(1 + 2\mathrm{SNR})}{N_t \pi^2 \mathrm{SNR}^2} \tag{28}$$

with the sampling interval being $T_s = 10$ ns and the sampling number N_t being τ/T_s, where $\tau = 1$ ms. The RMSE of estimated coefficients is defined by

$$\mathrm{RMSE} = \frac{1}{V}\sqrt{\sum_{v=1}^{V}((c_{1,v} - \hat{c}_{1,v})^2 + (c_{2,v} - \hat{c}_{2,v})^2)} \tag{29}$$

where V is the Monte Carlo time, $c_{i,v}$ is the true value of c_i in the vth Monte Carlo experiment ($i = 1, 2$) and $\hat{c}_{i,v}$ is the estimate of $c_{i,v}$. We set $V = 100$ in this paper.

As comparisons, the simulated methods include the norm-2 method, the SF method in [16], the RGS method in [11] and the MUSIC method in [21], where MUSIC utilizes the converted TDOA measurements $\exp(\sqrt{-1} \times 2\pi \tilde{\boldsymbol{d}}/(2 \max_{g,m} |d_{m,1}^g|))$ (Readers are referred to [20] for more details on the conversion of TDOA measurements). Additionally, the hyperparameter in SF is set to 0.1.

A. RMSE PERFORMANCE TESTS IN 2D GRID-SEARCH

In this subsection, G is set to 81. Thus the grid-points in the c_1 and c_2 axis are $[-0.1 : 0.025 : 0.1]$ and $[-0.1 : 0.025 : 0.1]$, respectively. In each Monte Carlo experiment, c_1 and c_2 are generated uniformly between -0.1 and 0.1.

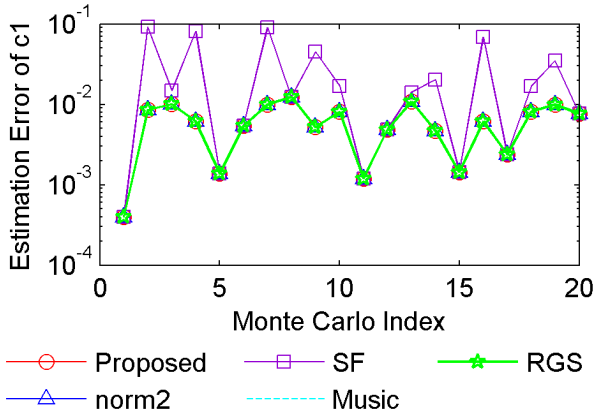

FIGURE 6. Absolute estimation error of coefficient c_1 with known H_1.

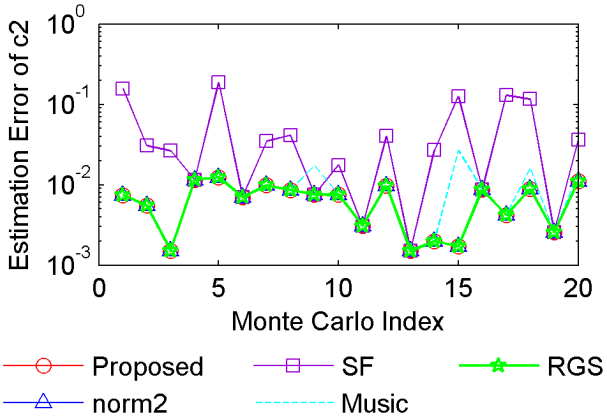

FIGURE 7. Absolute estimation error of coefficient c_2 with known H_1.

The absolute estimation errors of c_1 and c_2 versus different Monte Carlo experiment indexes are depicted in Fig. 6 and Fig. 7, respectively, with SNR fixed to 5 dB. It can be observed that SF behaves badly compared with other methods. The reason for this may be the poor restricted isotropy property (RIP) of the grid map. Other methods provide the similar coefficient recovery accuracies.

The SNR performances of the considered methods are given in Fig. 8. The results coincide with those of Fig. 6 and Fig. 7. Additionally, the RMSEs of the simulated methods other than SF are very close to RMSE(r). Hence, most methods are sufficient to select the NGP of $\boldsymbol{r}$ in 2D grid-search.

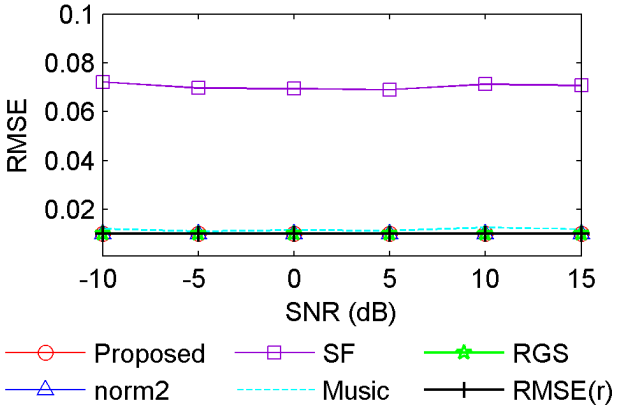

FIGURE 8. RMSE of coefficients versus SNR with known H_1.

B. RMSE PERFORMANCE TESTS IN 3D GRID-SEARCH

As the simulation conditions of this subsection, H_1 is unknown. Hence the range of H_1 is [100, 500] km. There are 10 grid-points in the c_1, c_2 and H_1 axis, respectively. Thus the grid-points in the c_1, c_2 and H_1 axes are $[-0.1 : 0.2/9 : 0.1]$, $[-0.1 : 0.2/9 : 0.1]$ and [100:400/9:500], respectively. Notably, the trick to build uniform grids has been given in Section III-A. In each Monte Carlo experiment, c_1 and c_2 are generated uniformly between -0.1 and 0.1; and H_1 is generated uniformly between 100 km and 500 km.

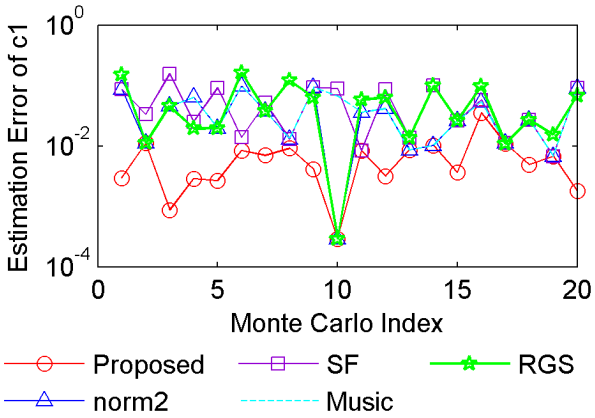

FIGURE 9. Absolute estimation error of coefficient c_1 with unknown H_1.

The absolute estimation errors of c_1 and c_2 versus different Monte Carlo indexes are depicted in Fig. 9 and Fig. 10, respectively, with SNR fixed to 5 dB. Different from the 2D grid-search scenario, the proposed method behaves much better than other methods for most Monte Carlo indexes. The performance of RGS degrades badly with the increase of dimension, which verifies the claim in Section II-C; and SF still behaves worse than other methods.

The SNR performances of the considered methods in 3D grid-search are given in Fig. 11. The results coincide with those of Fig. 9 and Fig. 10. Hence, the proposed method is superior to the current state-of-the-art in 3D grid-search.

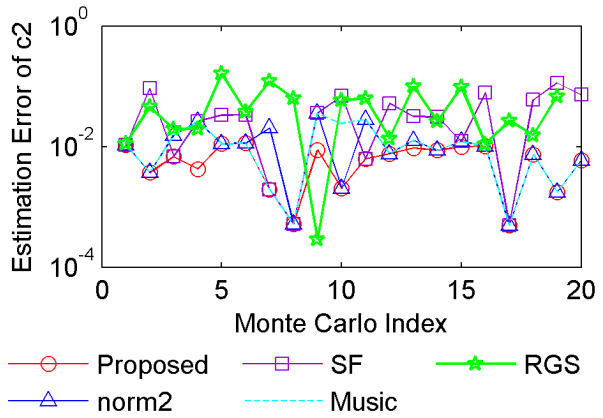

FIGURE 10. Absolute estimation error of coefficient c_2 with unknown H_1.

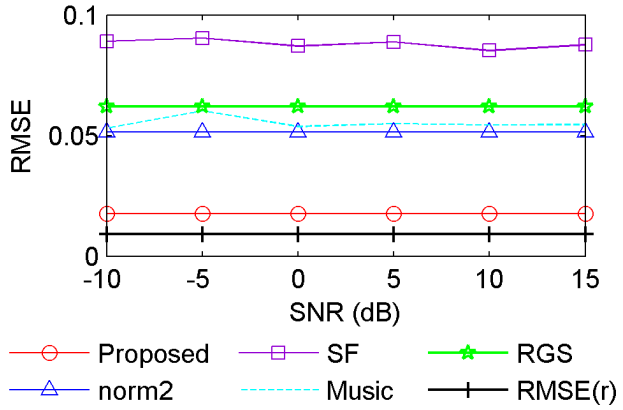

FIGURE 11. RMSE of coefficients versus SNR with unknown H_1.

C. IDENTITY-TEST PERFORMANCE IN 3D GRID-SEARCH

To evaluate the identity-test performance of the proposed method, false rejection rate P_R and false acceptance rate P_A are introduced in this subsection. P_R represents the percentage of wrongly judging the identical IVHs to be different; and P_A represents the percentage of wrongly judging the different IVHs to be identical.

As the simulation conditions, we set $G = 11^3$ (i.e., the grid number per axis is 11), leading to $c_1 = [-0.1 : 0.02 : 0.1]$, $c_2 = [-0.1 : 0.02 : 0.1]$ and $H_1 = [100{:}40{:}500]$ km.

To test the false rejection rate, we suppose that $H_1, \cdots, H_M$ are identical when $|c_1| \leq 0.01$ and $|c_2| \leq 0.01$ hold. Then we generate c_1 and c_2 uniformly within $[-0.01, 0.01]$ for 100 Monte Carlo experiments and suppose that a false rejection happens when $|\hat{c}_1| > 0.02$ or $|\hat{c}_2| > 0.02$, with $\hat{c}_i$ the estimate of c_i $(i = 1, 2)$. The false rejection rates are depicted in Fig. 12. Obviously, the proposed method leads to the least false rejection rate.

On the other hand, by uniformly generating c_1 and c_2 within $[-0.02, -0.01]$ and $[0.01, 0.02]$ for 100 Monte Carlo experiments, we suppose that a false acceptance happens when $\hat{c}_1 = \hat{c}_2 = 0$. The results are shown in Fig. 13. It is observed that the false acceptance rate is very small when

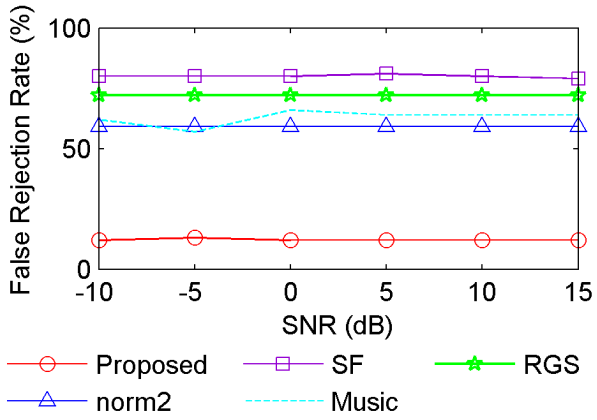

FIGURE 12. False rejection rate versus SNR with unknown H_1.

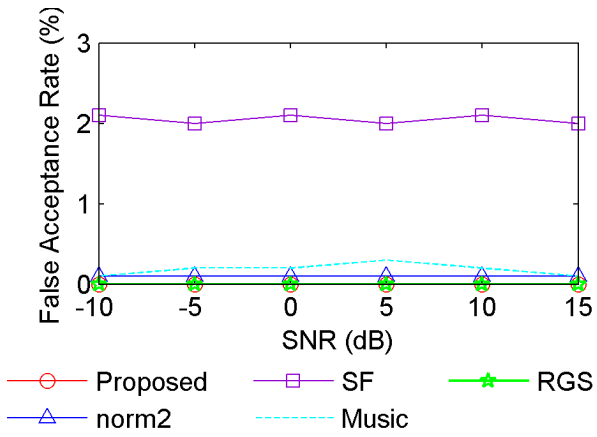

FIGURE 13. False acceptance rate versus SNR with unknown H_1.

methods other than SF are used; and the proposed method along with RGS provides the smallest false acceptance rate.

VI. CONCLUSION

In this paper, the identity-test problem of IVHs is studied. The inputs of this problem are TDOA measurements from a known-position target; and the identity-test of IVHs is realized by solving a coefficient retrieval problem. As the main contribution, an improved grid-search method is proposed. Compared with an existing novel grid-search method, the proposed method avoids the approximation that selecting the right hypersphere (where the unknown vector is located) is equivalent to selecting the NGP. This merit makes the proposed method superior to the current state-of-the-art in terms of recovery accuracy. Besides, the training phase and the searching phase of the proposed method are computationally cheap. Simulation results demonstrate the superiority of the proposed method when solving a 3D grid-search problem.

REFERENCES

[1] X. Li, Z. D. Deng, L. T. Rauchenstein, and T. J. Carlson, "Contributed review: Source-localization algorithms and applications using time of arrival and time difference of arrival measurements," *Rev. Sci. Instrum.*, vol. 87, no. 4, pp. 1–13, Apr. 2016.

[2] Y. T. Chan and K. C. Ho, "A simple and efficient estimator for hyperbolic location," *IEEE Trans. Signal Process.*, vol. 42, no. 8, pp. 1905–1915, Aug. 1994.

[3] Y.-T. Chan, H. Y. C. Hang, and P.-C. Ching, "Exact and approximate maximum likelihood localization algorithms," *IEEE Trans. Veh. Technol.*, vol. 55, no. 1, pp. 10–16, Jan. 2006.

[4] G. Mao, B. Fidan, and B. D. O. Anderson, "Wireless sensor network localization techniques," *Comput. Netw.*, vol. 51, no. 10, pp. 2529–2553, 2007.

[5] H. Hmam, "Optimal sensor velocity configuration for TDOA-FDOA geolocation," *IEEE Trans. Signal Process.*, vol. 65, no. 3, pp. 628–637, Feb. 2017.

[6] J. Li, F. Guo, L. Yang, W. Jiang, and H. Pang, "On the use of calibration sensors in source localization using TDOA and FDOA measurements," *Digit. Signal Process.*, vol. 27, pp. 33–43, Apr. 2014.

[7] G. Wang, A. M.-C. So, and Y. Li, "Robust convex approximation methods for TDOA-based localization under NLOS conditions," *IEEE Trans. Signal Process.*, vol. 64, no. 13, pp. 3281–3296, Jul. 2016.

[8] W. Wang, G. Wang, F. Zhang, and Y. Li, "Second-order cone relaxation for TDOA-based localization under mixed LOS/NLOS conditions," *IEEE Signal Process. Lett.*, vol. 23, no. 12, pp. 1872–1876, Dec. 2016.

[9] Z. Su, G. Shao, and H. Liu, "Semidefinite programming for NLOS error mitigation in TDOA localization," *IEEE Commun. Lett.*, vol. 22, no. 7, pp. 1430–1433, Jul. 2018.

[10] H. Geng, Y. Liang, F. Yang, L. Xu, and Q. Pan, "Joint estimation of target state and ionospheric height bias in over-the-horizon radar target tracking," *IET Radar, Sonar Navigat.*, vol. 10, no. 7, pp. 1153–1167, Aug. 2015.

[11] T.-N. Zhang, X.-P. Mao, C.-L. Zhao, and J.-X. Liu, "A novel grid selection method for sky-wave time difference of arrival localisation," *IET Radar, Sonar Navigat.*, vol. 13, no. 4, pp. 538–549, Apr. 2019.

[12] R. J. Norman and P. L. Dyson, "HF radar backscatter inversion technique," *Radio Sci.*, vol. 41, pp. 1–10, Aug. 2006.

[13] H. Jamali-Rad and G. Leus, "Sparsity-aware multi-source TDOA localization," *IEEE Trans. Signal Process.*, vol. 61, no. 19, pp. 4874–4887, Oct. 2013.

[14] Z. Tan, P. Yang, and A. Nehorai, "Joint sparse recovery method for compressed sensing with structured dictionary mismatches," *IEEE Trans. Signal Process.*, vol. 62, no. 19, pp. 4997–5008, Oct. 2014.

[15] Z. Yang, L. Xie, and C. Zhang, "Off-grid direction of arrival estimation using sparse Bayesian inference," *IEEE Trans. Signal Process.*, vol. 61, no. 1, pp. 38–43, Jan. 2013.

[16] C. R. Comsa, A. M. Haimovich, S. C. Schwartz, Y. H. Dobyns, and J. A. Dabin, "Time difference of arrival based source localization within a sparse representation framework," in *Proc. 45th Annu. Conf. Inf. Sci. Syst.*, Mar. 2011, pp. 1–6.

[17] Y. Zhou, H. Leung, and P. C. Yip, "An exact maximum likelihood registration algorithm for data fusion," *IEEE Trans. Signal Process.*, vol. 45, no. 6, pp. 1560–1573, Jun. 1997.

[18] Z.-Q. Luo, W.-K. Ma, A. M.-C. So, Y. Ye, and S. Zhang, "Semidefinite relaxation of quadratic optimization problems," *IEEE Signal Process. Mag.*, vol. 27, no. 3, pp. 20–34, May 2010.

[19] F. K. W. Chan, H. C. So, W.-K. Ma, and K. W. K. Lui, "A flexible semidefinite programming approach for source localization problems," *Digit. Signal Process.*, vol. 23, pp. 601–609, Mar. 2013.

[20] T.-N. Zhang, X.-P. Mao, Y.-M. Shi, and G.-J. Jiang, "An analytical subspace-based robust sparse Bayesian inference estimator for off-grid TDOA localization," *Digit. Signal Process.*, vol. 69, pp. 174–184, Oct. 2017.

[21] W.-Q. Wang and H. C. So, "Transmit subaperturing for range and angle estimation in frequency diverse array radar," *IEEE Trans. Signal Process.*, vol. 62, no. 8, pp. 2000–2011, Apr. 2014.

[22] M. Zhao, X. Zhang, Q. Yang, and W. Deng, "Using sky-wave echoes information to extend HFSWR's maximum detection range," *Radio Sci.*, vol. 53, no. 8, pp. 922–932, Aug. 2018.

[23] Q. He, X. Li, Z. He, and R. S. Blum, "MIMO-OTH radar: Signal model for arbitrary placement and signals with non-point targets," *IEEE Trans. Signal Process.*, vol. 63, no. 7, pp. 1846–1857, Apr. 2015.

[24] D. Bourgeois, C. Morisseau, and M. Flecheux, "Over-the-horizon radar target tracking using multi-quasi-parabolic ionospheric modelling," *IEE Proc.-Radar, Sonar Navigat.*, vol. 153, no. 5, pp. 409–416, Oct. 2006.

[25] W. H. Foy, "Position-location solutions by Taylor-series estimation," *IEEE Trans. Aerosp. Electron. Syst.*, vol. AES-12, no. 2, pp. 187–194, Mar. 1976.

[26] X. Chen, D. Wang, J. Yin, and Y. Wu, "Performance analysis and dimension-reduction Taylor series algorithms for locating multiple disjoint sources based on TDOA under synchronization clock bias," *IEEE Access*, vol. 6, pp. 48489–48509, 2018.

[27] H. C. So, Y. T. Chan, and F. K. W. Chan, "Closed-form formulae for time-difference-of-arrival estimation," *IEEE Trans. Signal Process.*, vol. 56, no. 6, pp. 2614–2620, Jun. 2008.

TIE-NAN ZHANG received the B.S. and M.S. degrees from the Harbin Institute of Technology, in 2008 and 2014, respectively, where he is currently pursuing the Ph.D. degree in information and communication engineering. His research interests include sky-wave passive radar and time-difference-of-arrival localization.

XING-PENG MAO received the B.S. degree in radio electronics from Northeast Normal University, China, in 1993, and the M.S. and Ph.D. degrees in communication and information system from the Harbin Institute of Technology, China, in 1999 and 2004, respectively. His research interests include array signal processing, communication and radar system design, and the theory on advanced radar systems.

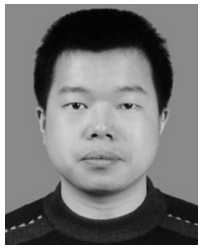

YU-GUAN HOU received the M.S. and Ph.D. degrees in communication and information system from the Harbin Institute of Technology, China, in 2003 and 2008, respectively. His research interests include array signal processing and statistical signal processing.

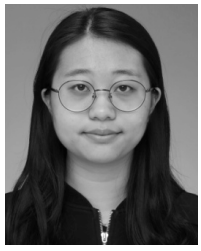

HE MA was born in Dalian, Liaoning, China, in 1996. She received the B.S. degree in communication engineering from Dalian Maritime University, in 2018. She is currently pursuing the M.S. degree in information and communications engineering and the Ph.D. degree with the Harbin Institute of Technology. Her main research interest includes sky-wave time-difference-of-arrival localization technology.